ORIGINAL PAPER

Temporal and spatial evolution of the standard precipitation evapotranspiration index (SPEI) in the Tana River Basin, Kenya

Francis Polong [1,2] · Haishan Chen [1] · Sanlei Sun [1] · Victor Ongoma [3]

Abstract

The focus of this paper was to investigate the spatial and temporal variability of dry and wet events using the standard precipitation and evapotranspiration index (SPEI) in the Tana River Basin (TRB) in Kenya. The SPEI is a new drought index which incorporates the effect of evapotranspiration on drought analysis thus making it possible to identify changes in water demand in the context of global warming. The SPEI was computed at 6- and 12-month timescales using a 54-year long monthly rainfall data from the Global Precipitation and Climate Center (GPCC) and temperature data from the Climate Research Unit (CRU) both recorded between 1960 and 2013. Both datasets have a spatial resolution of 0.5° by 0.5° and were extracted for every grid point in the basin. The SPEI was used to assess the temporal and spatial evolution of dry and wet events as well as determine their duration, severity, and intensity. The evolution of significant historical dry and wet events and the frequency of occurrence were clearly identified. The index showed that the period between 1960 and 1980 was dominated by dry events while wet events were dominant in the period between 1990 and 2000. The SPEI6 had the longest duration of dry events of 30 months and severity of 44.67 which was observed at grid 5while the highest intensity was 2.18 observed at grid 31. Grid 19 had the longest duration (52 months) and highest severity (88.08) of dry events for SPEI12 and the intensity was highest (1.94) in grid 31. The longest duration (23) and highest severity (40.03) of wet events for SPEI6 were recorded in grid 39. The highest intensity of wet events for SPEI6 was 1.91 at grid 23 and 1.81 at grid 37 for SPEI12. The principal component analysis (PCA) was applied to the SPEI time series in order to assess the spatial pattern of variability of the dry and wet events in the basin. The PCA showed that there were two leading components which explained over 80% of the spatial variation of dry and wet events in the basin. Further, the continuous wavelet transform (CWT) was applied to the PCA scores in order to capture the time-frequency dynamics. The wavelet transform of the SPEI6 and SPEI12 identified significant periodicities of 1 to 2 years across the spectrum.

1 Introduction

Currently, there is great concern that climate change coupled with human-induced environmental degradation is a major threat to contemporary water resources management in the world (Githui et al. 2009; Huang et al. 2012). Many studies have indicated that global warming alters the patterns of rainfall resulting into more frequent extreme weather events such as droughts and floods (Zhang et al. 2009). Climate models predict that climate change is expected to increase the risk of drought in some areas of the world and the risk of extreme precipitation and flooding in others (IPCC 2007).

Kenya has frequently witnessed prolonged and severe droughts leading to electric power and water rationing with negative impacts on the economy (The World Bank 2011). Power rationing and reduction in water supplies (especially to Nairobi and the environs) have been attributed to a reduction in available surface water resources in the TRB (Nakaegawa and Wachana 2012). Moreover, increasing water demands lead to conflicts among competing water users that are mostly pronounced during drought periods (Hisdal and Tallaksen 2003; Santos et al. 2010). Studies have shown that

✉ Francis Polong
   fl_pol@yahoo.com

1   Key Laboratory of Meteorological Disaster, Ministry of Education (KLME)/International Joint Research Laboratory of Climate and Environment Change (ILCEC)/Collaborative Innovation Center on Forecast and Evaluation of Meteorological Disasters (CIC-FEMD), Nanjing University of Information Science and Technology (NUIST), Nanjing 210044, China

2   Kenya Industrial Research and Development Institute, P.O. Box 30650-00100, Nairobi, Kenya

3   Department of Meteorology, South Eastern Kenya University, P.O. Box 170-90200, Kitui, Kenya

drought in the country affects more than 3.7 million people and its combined economic impact and related shocks run into 100 s of millions of dollars (The World Bank 2011). Recently, there have been debates on the apparent increase in intensity and frequency of drought and its possible causes. Even though projections by climate models depict a scenario of increase in rainfall in the East African region (IPCC 2007), recent studies (e.g., Rowell et al. 2015; Lyon and Dewitt 2012; Shongwe et al. 2011; Liebmann et al. 2014; Lyon 2014; Ongoma and Chen 2017) have shown a decline in temporal and spatial distribution of rainfall in the region which has led to increased intensity and frequency of drought. Some authors have attributed the drought condition to climate change effects caused by the emission of anthropogenic greenhouse gases into the atmosphere (Williams and Funk 2011). This may increase the uncertainty in the availability of surface water in Kenya especially because of the existing water scarcity problem coupled with the high demand for agriculture, industry, and the burgeoning population (Nakaegawa and Wachana 2012). Hence, the assessment of climate variability in terms of dry and wet events may contribute to a more prudent monitoring of climate-related risks and develop appropriate adaptation and mitigation strategies (Hayes et al. 2005).

The TRB is a vital resource for socio-economic development of Kenya and for the sustenance and preservation of ecological systems in the basin. It supplies about 95% of the water needs of the capital city of Nairobi and contributes 65–75% of the hydropower production in the country (Baker et al. 2015; Oludhe et al. 2013; Jacobs et al. 2007; Gichuki and Vigerstol 2014). Recently, the government has put in place significant development targets for hydropower, domestic water provision, and irrigated agriculture in the basin as part of the Vision 2030 development plan (Baker et al. 2015). However, the basin has been experiencing frequent hydrological extremes in terms of droughts and floods which have been attributed to climate change and environmental degradation (Nakaegawa and Wachana 2012). A recent study by Kerandi et al. (2016) concluded that precipitation over the TRB has generally been decreasing since the 1997/1998 El Niño rains in Kenya, with 2011 to 2014 recording below normal mean annual precipitation. This means that the increasing water demand in the TRB coupled with climate variability is exerting a lot of pressure on the water resources of the basin. Therefore, it is crucial for water resource managers and developers to understand how climate variability, on both long and short timescales, will affect water availability. This further reinforces the need for studies that will attempt to understand the possible consequences of climate change processes on the future availability of water resources in the basin and to determine the current relationship between climate variability and water resources. In this regard, the significance of a drought index such as the SPEI would be its applicability in drought monitoring, risk assessment and planning, and management of water resources of the TRB.

There are a number of quantitative drought indices that have been proposed by the research fraternity for assessing the severity of droughts in regard to water resources planning and risk assessment (Burke et al. 2006; Gao et al. 2017). Among these indices is the recently developed SPEI which is an improved drought index well suited for studies of the effect of global warming on drought severity (Vicente-Serrano et al. 2010). The SPEI is good at detecting, monitoring, and exploring the consequences of global warming on drought conditions (Dubrovsky et al. 2009). The SPEI is superior to other widely used drought indices and it is capable of identifying the role of evapotranspiration and temperature variability with regard to drought assessment in the context of global warming (Vicente-Serrano et al. 2010; Potop et al. 2012; Wu et al. 2016). Furthermore, it is now well known that although the primary cause of drought is rainfall deficiency, temperature plays an important role in initiating drought (Shi et al. 2017; Chen and Sun 2015). Due to this, the SPEI has been recommended as an alternative to other drought indices to quantify anomalies in accumulated climatic water balance, incorporating potential evapotranspiration (Stagge and Tallaksen 2014). A number of studies have investigated the occurrence of drought using the SPEI. Yu et al. (2014) calculated the SPEI based on monthly precipitation and air temperature values and found an increase in severe and extreme droughts for the whole of China. Potop et al. (2012) used the SPI and SPEI to study the evolution of secular drought from 1901 to 2010 in the lowland regions of the Czech Republic. Their study explored the relationship between extreme dry and extreme wet episodes with vegetable yields in the lowland regions of the Czech Republic and found that more than 40% of the months during the vegetable-growing season can be affected by moderate and severe drought. Lorenzo-Lacruz et al. (2010) applied the SPI and SPEI to analyze the influence of climate variation on the availability of water resources in the headwaters of the Tagus River basin. Among their findings was that the responses in river discharge and reservoir storage were slightly higher when based on the SPEI rather than the SPI, indicating that although precipitation had a major role in explaining temporal variability in the analyzed parameters, the influence of temperature was not negligible. Chen and Sun (2015) in their study of drought characteristics over China found differences in the estimates of SPEI calculated using different evapotranspiration parameterizations. Vicente-Serrano et al. (2012) compared the performance of several drought indices for ecological, agricultural, and hydrologic studies and concluded that SPEI was the best index to capture the effects of summer droughts. Moreover, a recent study on temperature and precipitation variability over the East African region by Ongoma and Chen (2017) showed that there has been an increase in temperature in the region with significant positive changes observed from the year 1992.

The goal of this study is to determine the historical and recent climatic variability in the TRB based on the assessment of spatial and temporal variability of dry and wet events in the basin. Specifically the study will (1) analyze the temporal and spatial evolution and variation of the SPEI over the basin, (2) use the PCA to identify the spatial and temporal patterns of dry and wet events, and (3) apply continuous wavelet transform to identify cycles of dry and wet events in the temporal patterns. To the best of our knowledge, no other study of this kind has been conducted in the region and thus it will go a long way in contributing to the body of literature in the region. Further, the study is intended to be used for drought monitoring, risk assessment, and water resources planning. The major challenge to prudent risk management approaches is the lack of reliable and updated climatological records that are suitable for risk analysis (Raziei et al. 2011; Hayes et al. 2005). Data availability is the most important limitation that hinders establishing a drought monitoring and early warning system in developing countries (Worqlul et al. 2014). To overcome this obstacle, this study used high spatial resolution gridded datasets from the GPCC (rainfall) and the CRU (temperature) for the analysis of dry and wet events in the TRB.

2 Data and methodology

2.1 Study area

The TRB lies between the latitudes 0° 0′ 53″ S and 3° 0′ 00″ S and between the longitudes 37° 00′ 00″ E and 41° 00′ 00″ E. The basin is marked by a complex terrain with a very steep topography which rises from sea level in the coastal plains along the Indian Ocean to over 5000 m above sea level in Mount Kenya (Fig. 1). The size of the basin ranges between 100,000 and 126,000 km^2 (Baker et al. 2015). The Tana River which forms the basin is the longest river in Kenya at approximately 1000 km. Its headwaters are on Mt. Kenya and the Aberdare Range and winds through a densely forested ecosystem to agricultural and rangeland areas and ultimately discharging into the Indian Ocean (Okazawa et al. 2009). The river is a vital resource for the socio-economic development of the country and is important for the sustenance and preservation of ecological systems in the basin. The basin is the source of about 95% of the water needs of the capital city of Nairobi and is also a major source of hydropower and irrigation-fed agriculture production in Kenya (Baker et al. 2015). The basin has a varied climate ranging from humid in the highlands to arid and semi-arid in the lowlands, with a close correlation of elevation and climatic zones. Rainfall characteristics are primarily influenced by topography and the proximity to the Indian Ocean (Kerandi et al. 2016). The long-term annual average and long-term monthly average distribution of rainfall and long-term monthly average minimum and maximum temperature in the basin is given in Fig. 2.

2.2 Data

This study utilized the monthly gridded rainfall data at 0.5° × 0.5° resolution for 54 years (1960–2013) covering the entire TRB acquired from the Global Precipitation and Climate Center (GPCC) version 7 (http://gpcc.dwd.de). The temperature data that was used for calculating potential evapotranspiration was acquired from the CRU dataset based on a similar resolution as the rainfall data. The GPCC provides an updated and globally gridded precipitation estimate extracted from surface rain gauge observations with a minimum of 90% data availability over the years 1951–2000. The GPCC Reanalysis (V7) for the period 1901 to 2013 is based on quality-controlled data from all stations in GPCC's database. This product is optimized for best spatial coverage and is recommended for water-budget studies (Schneider et al. 2014). The gridded reanalysis data were adopted as a substitute to the scarce rain gauge climatological data. A simple evaluation of the GPCC and CRU datasets with the observed rainfall data measured at six (6) World Meteorological Organization synoptic stations within the basin showed that GPCC had higher positive correlation of above 0.9 in all the stations and therefore the GPCC data was used for rainfall, and CRU data was solely used for temperature-based derivation of potential evapotranspiration. Gridded rainfall data have been widely used in various hydroclimatological analyses in different parts of the world (Rajeevan et al. 2006; Caramelo and Orgaz 2007; Jury 2010; Raziei et al. 2011; Mahfouz et al. 2016). Jury (2010) used 0.5° × 0.5° gridded precipitation data for the period between 1901 and 2007 from the GPCC dataset to study decadal climate variability in Ethiopia. Likewise Wagesho et al. (2013) successfully used the GPCC data to determine the temporal and spatial variability of annual and seasonal rainfall over Ethiopia. In this study, the gridded data was extracted from 43 grid cells within the basin as shown in Fig. 1.

2.3 Methodologies

2.3.1 Calculation of the SPEI

SPEI is a drought index based on precipitation and PET, which describes the degree of deviation of dry and wet conditions by standardizing the difference between PET and precipitation. It can describe water deficit effectively with multiple timescales, reflecting the lag relation between different water resources, precipitation, and evapotranspiration (Liu et al. 2015). The SPEI is calculated using the difference between monthly (or weekly) precipitation and potential evapotranspiration data which is aggregated over the time period and fitted to a probability distribution function (Vicente-serrano et al. 2010). The difference between precipitation and evapotranspiration (i.e.,
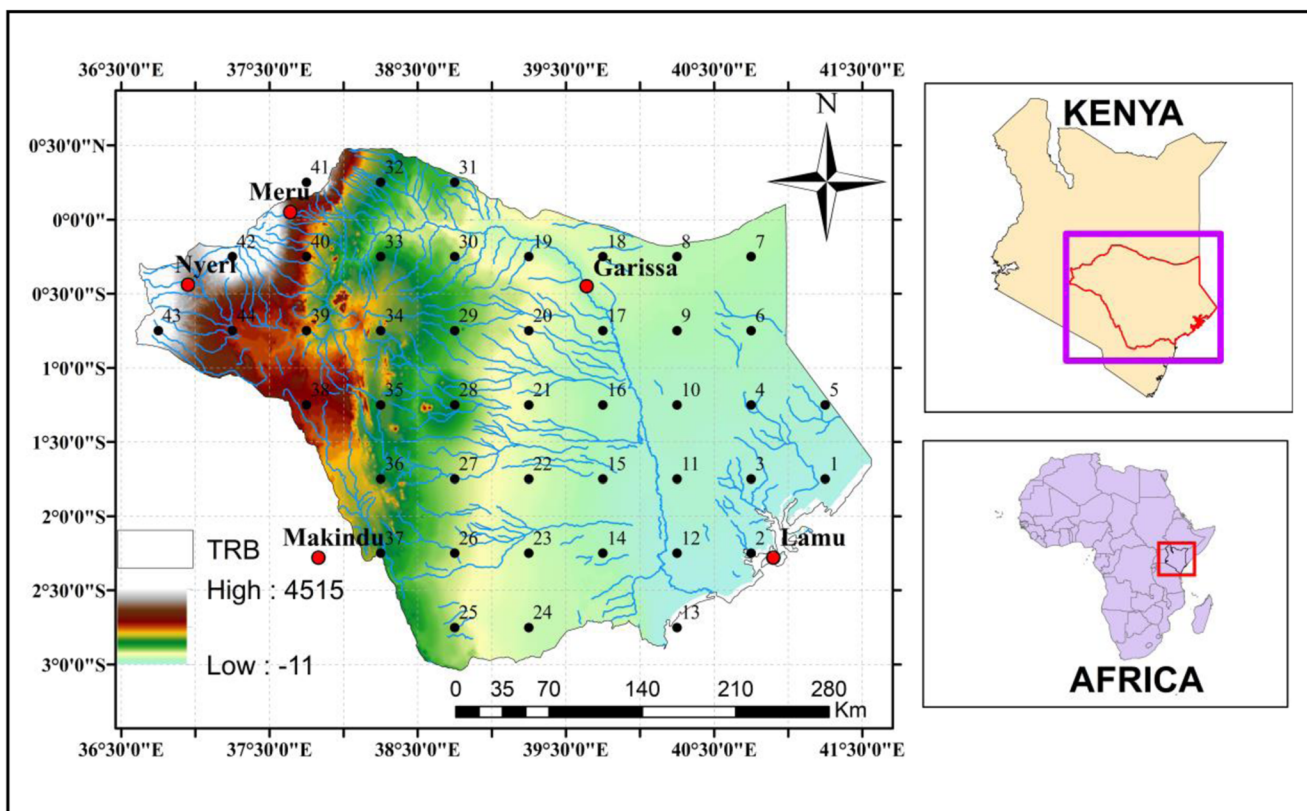
Fig. 1 The map of the study area showing the topography, the location of the meteorological stations, and the sampled grid cells in the TRB

moisture deficit) can be negative and is commonly so in semi-arid and arid regions and therefore, a three-parameter distribution is needed to model the deficit values (Hernandez and Uddameri 2014). The log-logistic three-parameter distribution is commonly applied as it fits the extreme values better, and the fitted cumulative probability density function is transformed to the standard normal distribution, which is also the SPEI (Vicente-Serrano

et al. 2010; Zambreski 2016). Positive values of SPEI indicate above average moisture conditions while negative values indicate below normal (dry) conditions.

In this study, the SPEI values are calculated for 6- and 12-month timescales for each grid cell. Calculations were performed using the "SPEI package" available in R-program (Beguería and Vicente-Serrano 2013). The calculation of the SPEI is briefly described as follows;
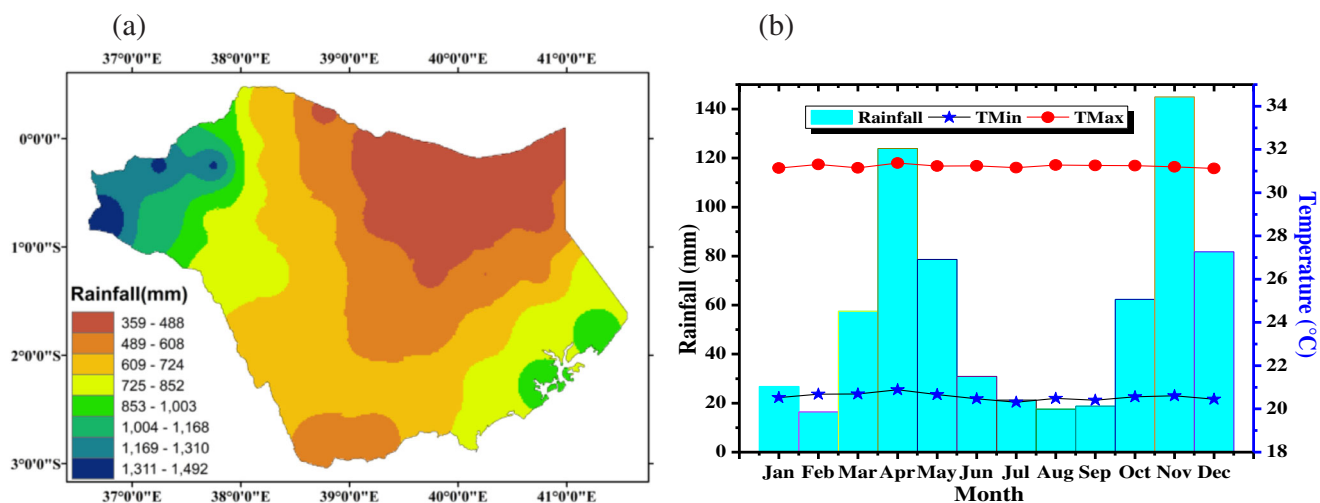

Fig. 2 The spatial and temporal patterns of annual mean rainfall, minimum, and maximum temperature over the basin (1960–2013)

(1) Calculate the difference between precipitation and PET on monthly basis (Eq. 1);

$$D_j = P_j - PET_j \qquad (1)$$

The PET was calculated using the Hargreaves equation which has limited data requirements and does not suffer the inherent limitations of the Thornthwaite equation and it performs relatively close to the standard FAO PM equation (Beguería et al. 2014; Droogers and Allen 2002; Hargreaves and Allen 2003).

(2) The next step is to calculate the accumulated difference between precipitation and PET at different timescales. The accumulated difference $\left(X_{i,j}^k\right)$ at the k-month timescale is calculated using Eq. 2;

$$\begin{cases} X_{i,j}^k = \sum\limits_{l=13-k+j}^{12} D_{i-1,l} + \sum\limits_{l=1}^{j} D_{i,j} & if \quad j \vartriangleleft k \\ X_{i,j}^k = \sum\limits_{i=j-k+1}^{j} D_{i,j} & if \quad j \geq k \end{cases} \qquad (2)$$

where $X_{i,j}^k$ is the accumulated difference between precipitation and the PET at the k-month timescale in the j-month of the i-th year; $D_{i,l}$ is the monthly difference between the precipitation and the PET in the l-month of the i-th year.

(3) Normalize the $X_{i,j}^k$ data sequence. Because there may be negative values in the original data sequence $X_{i,j}^k$, therefore, the SPEI uses the three-parameter log-logistic probability distribution (Vicente-Serrano et al. 2010). For the data sequence of all timescales, the accumulative function of the log-logistic probability distribution $F(X)$ is as given in Eq. 3;

$$F(X) = \left[1 + \left(\frac{\alpha}{x-\gamma}\right)^{\beta}\right]^{-1} \qquad (3)$$

where α, β, and γ are scale, shape, and position parameters, respectively, which can be calculated using the equations proposed by Vicente-Serrano et al. (2010).

p is the probability of a definite $X_{i,j}^k$ value:

$$p = 1 - F(X) \qquad (4)$$

If $p \leq 0.5$,

$$w = \sqrt{-2\ln p} \qquad (5)$$

$$SPEI = w - \frac{C_0 + C_1 w + C_2 w^2}{1 + d_1 w + d_2 w^2 + d_3 w^3} \qquad (6)$$

If $p > 0.5$,

$$w = \sqrt{-2\ln(1-p)} \qquad (7)$$

$$SPEI = \frac{C_0 + C_1 w + C_2 w^2}{1 + d_1 w + d_2 w^2 + d_3 w^3} \qquad (8)$$

where $C_0 = 2.515517$, $C_1 = 0.802853$, $C_2 = 0.010328$, $d_1 = 1.432788$, $d_2 = 0.189269$, and $d_3 = 0.001308$ (Gao et al. 2017).

The calculated values of the SPEI are classified as shown in Table 1 and are used to analyze for the characteristics of dry and wet events in the basin in terms of the duration, severity, intensity, and frequency of occurrence of dry and wet events. The duration of an event is the length of time (months) that the SPEI is consecutively at or below a truncation level. In this study, the threshold used for the SPEI ≤ -1 for dry event and SPEI ≥ 1 for wet event. The frequency is the number of months that the SPEI value meets a set value (Table 1) divided by the number of months in the entire series. The severity and intensity were calculated for all the grid cells sampled according to Zambreski (2016) as shown below:

(i) Severity is the cumulative sum of the index value based on the duration extent

$$S = \sum\limits_{i=1}^{Duration} Index \qquad (9)$$

(ii) Intensity of an event is the severity divided by the duration. Events that have shorter duration and higher severities will have large intensities.

$$I = \frac{Severity}{Duration} \qquad (10)$$

Table 1 Classification of the severity of dry and wet events based on the calculated SPEI

Category	SPEI value
Extreme dryness	Less than -2
Severe dryness	-1.99 to -1.5
Moderate dryness	-1.49 to -1.0
Near normal	-0.99 to 0.99
Moderate wetness	1.0 to 1.49
Severe wetness	1.5 to 1.99
Extreme wetness	More than 2.0

2.3.2 Principal component analysis

The principal component analysis (PCA) is a common way of identifying patterns in climatic data and expressing the data in such a way as to highlight their similarities and differences (Santos et al. 2010; Zhao et al. 2012). It is basically a data reduction method, which explains the correlation among several random uncorrelated variables in terms of a small number of underlying factors or principal components without extreme loss of information. This study uses the PCA to capture the spatial patterns of co-variability of dryness/wetness based on SPEI series at each grid cell. The original inter-correlated SPEI variables at different grid cells are $X_{i,\,1}, X_{i,\,2}, ..., X_{i,\,k}$ where k is the number of the grid cells in the basin (=43) and i represents the length of SPEI series at each grid cell. The principal components (PCs) are produced for the same time $Y_{i,\,1}, Y_{i,\,2}, ..., Y_{i,\,k}$ using linear combinations of the first ones according to Eq. 9;

$$\begin{cases} Y_{i,1} = a_{11}X_{i,1} + a_{12}X_{i,2} + \ldots + a_{1k}X_{i,k} \\ Y_{i,2} = a_{21}X_{i,1} + a_{22}X_{i,2} + \ldots + a_{2k}X_{i,k} \\ \qquad\qquad\qquad \vdots \\ Y_{1,k} = a_{k1}X_{i,k} + a_{k2}X_{i,2} + \ldots + a_{kk}X_{i,k} \end{cases} \qquad (11)$$

In the combination, the Y values are orthogonal and an uncorrelated variable, such that $Y_{i,\,1}$ explains most of the variance, $Y_{i,\,2}$ explains the remainder and so on. The coefficients of the linear combinations are called "loadings" and represent the weights of the original variables in the PCs (Santos et al. 2010). A detailed methodology of the PCA procedure is abundant in the literature (e.g., Santos et al. 2010; Bordi et al. 2004).

2.3.3 Wavelet transform analysis

Wavelet transform is a powerful method to characterize the frequency, intensity, time position, and duration of the variations in a climate data series by revealing the localized time and frequency information (Zhao et al. 2012). The wavelet transform can be used to analyze time series that contain non-stationary power at many different frequencies (Torrence and Compo 1998; Santos and Ideião 2005). The wavelet transform has been widely applied to the fields of climatic and hydrological changes. The wavelet transform was computed using the "WaveletComp" package available in R-program (Rosch and Schmidbauer 2014).

In the continuous wavelet transform, it is assumed that X_n is the time series with equal time interval Δt (1 month in this study). One particular wavelet, the Morlet, is defined as presented in Eq. 10;

$$\psi_0(n) = \pi^{-1/4}e^{i\omega_0\eta}e^{-\eta^2/2} \qquad (12)$$

where ω_0 is the dimensionless frequency and η denotes the non-dimensional time frequency (Torrence and Compo 1998; Zhao et al. 2012). The continuous wavelet transform of a discrete sequence X_n is defined as the convolution of X_n with a scale and translated version of $\varphi_0(n)$:

$$W_n(s) = \sum_{n'}^{N-1} X_n\psi^*\left[\frac{(n'-n)\delta t}{s}\right] \qquad (13)$$

where the asterisk represents the complex conjugate, s is the dilation parameter used to change the scale, and n is the translation parameter. By varying the wavelet scale s and translating along the localized time index n, one can construct a picture showing both the amplitude of any features versus the scale and how this amplitude varies with time (Torrence and Compo 1998).

The significance of wavelet power can be assessed relative to the null hypothesis that the signal is generated by a stationary process with a given background power spectrum. The distinctive red noise characteristics of the time series are modeled by a first-order auto-regressive process. Torrence and Compo (1998), and Lau and Weng (1995) give detail description of wavelet transform analysis. Significance testing of the wavelet transform is based on the assumption that the time series has a mean power spectrum and the significance of a peak in the wavelet power spectrum in relation to the background spectrum is used to determine the confidence level regarding the evaluation of potential periodicities (Hartmann et al. 2012). In this study, the periodicities were analyzed with a confidence level of 90%.

3 Results and discussion

3.1 Temporal evolution and frequency of occurrence of dry and wet events in the basin

The time series of the SPEI at 6- and 12-month timescales were calculated using a 54-year-long series of rainfall and temperature data (1960–2013) over 44 grid cells in the basin. Figure 3 shows the evolution of the SPEI for 6- and 12-month timescales averaged over all the grid cells in the TRB. The evolution of the mean SPEI over different parts of the TRB with similar climatic and physiographic features was computed and is shown in Fig. 4. It is evident that the shorter timescale (SPEI6) showed a higher temporal frequency of dry and wet events but the temporal frequency stabilizes for the 12-month timescale. This shows that the SPEI at a longer timescale responds more slowly and coherently to changes in monthly rainfall and temperature revealing clear periods of annual and multiple year dry and wet events. This means that longer timescales are better suited for the detection of historically significant events while shorter timescales show the frequent seasonal and inter-annual variations (Łabedzki 2007). It is seen that there are three contrasting
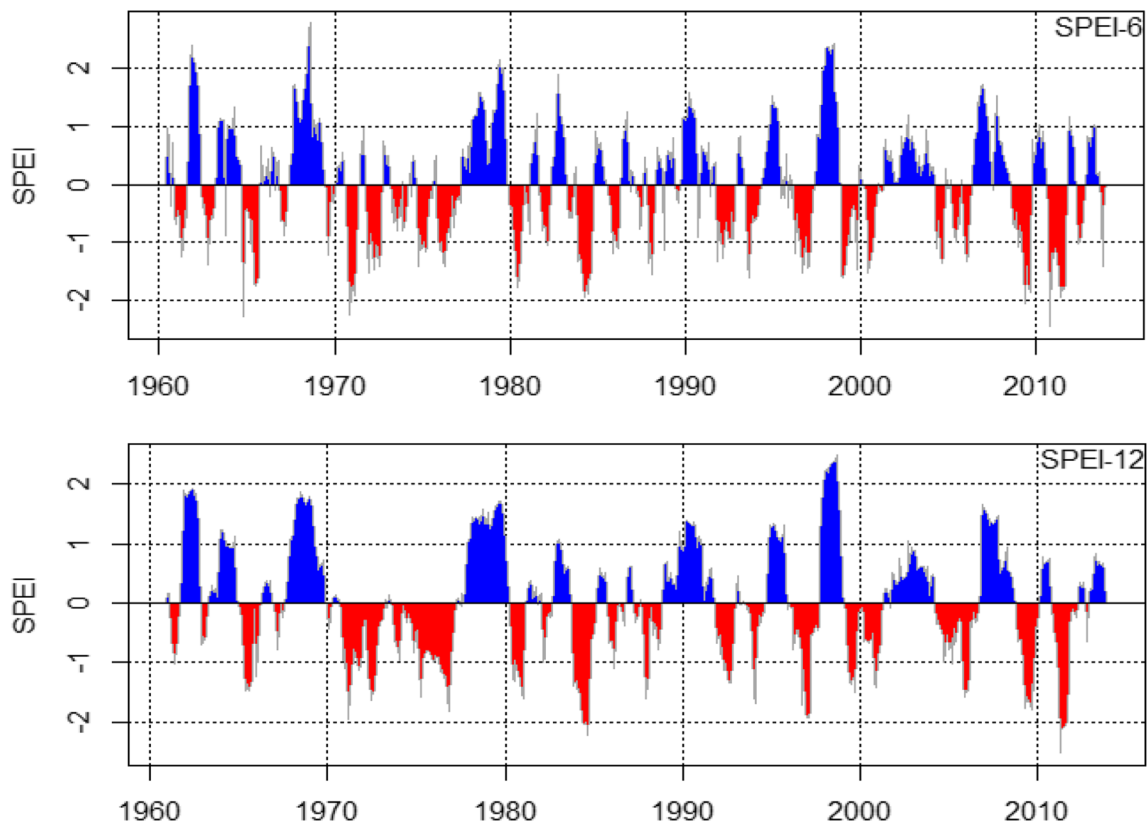
Fig. 3 The evolution of the mean SPEI for 6- and 12-month timescale over the TRB showing the variation in the duration, severity and intensity of dry and wet events

periods in the evolution of dry and wet events for both the 6- and 12-month SPEI. The dry events dominated the period between 1960 and 1980 while the wet events were dominant from 1980 to the later part of the 1990s even though there was a mix of both dry and wet events between the late 1990s and 2000s (although dry events were evidently dominant). Both timescales showed that the 1970s had the longest duration of dry events (consecutive negative SPEI values) implying that the dry events were dominant. The SPEI was able to identify some of the documented major drought and flood episodes in Kenya (e.g., 1964–1965, 1973–1974, 1983–1984, 1999–2000 and 2009–2011 (for drought), and 1978–1979 and 1997–1998 (for floods)) (Wambua et al. 2015; Mwale and Gan 2004). The driest month for both timescales of SPEI was recorded in grid cell 31 which occurred in August 1971 while the wettest month occurred in March 1998 in grid cell 7. In general, the wettest period was between 1997 and 1998 in the entire basin clearly showing the effects of the El Niño rainfall that were experienced during that period. It can be seen from the variations in the occurrence of dry and wet events that the basin is prone to hydrological extremes in terms of both drought and floods during the study period. The SPEI is able to clearly indicate the onset and cessation of a dry and/or wet event and this is found to vary from one grid cell to the other and also from one timescale to the other. Tables 2 and 3 show the duration, severity, and intensity of

occurrence of some of the major dry and wet events. The duration (persistence) of dry/wet event is given by the cumulative time that the SPEI is consecutively greater or less than a designated truncation value. In this study, the threshold value for dry event is SPEI ≤ -1 and SPEI ≥ 1 for wet event. The severity of an event is the cumulative sum of the index value based on duration extent while the intensity of an event is the event severity divided by the event duration (Zambreski 2016) as given in Eqns. 9 and 10. The longest duration of dry events for SPEI6 was 25 months which was observed in grid cells 18 and 19 while for that for SPEI12 was 52 months observed in grid cell 19. The longest duration of wet events for SPEI6 was 23 months observed in grid cells 13 (May 1982–March 1984) and 39 (Dec 1988–Oct 1990) while for SPEI12, the longest duration was observed in grid cell 21 and 39 between November 1992 and January 1996. It can be seen in Table 2 that the most severe dry event for SPEI6 was observed in grid cell 31 while for SPEI12 it occurred in grid cell 19. The most intense event was observed in grid cell 31 for both SPEI6 and SPEI12. As shown in Table 3, the most severe wet event occurred in grid cell 39 between December 1988 and October 1990 and had a magnitude of 40.03. For SPEI12, the most severe wet event occurred in grid cell 21 (Nov 1992-Jan 1996) with a magnitude of 57.22.

Usually, the extreme dry and wet events are the representative indicators of a changing climate and are the
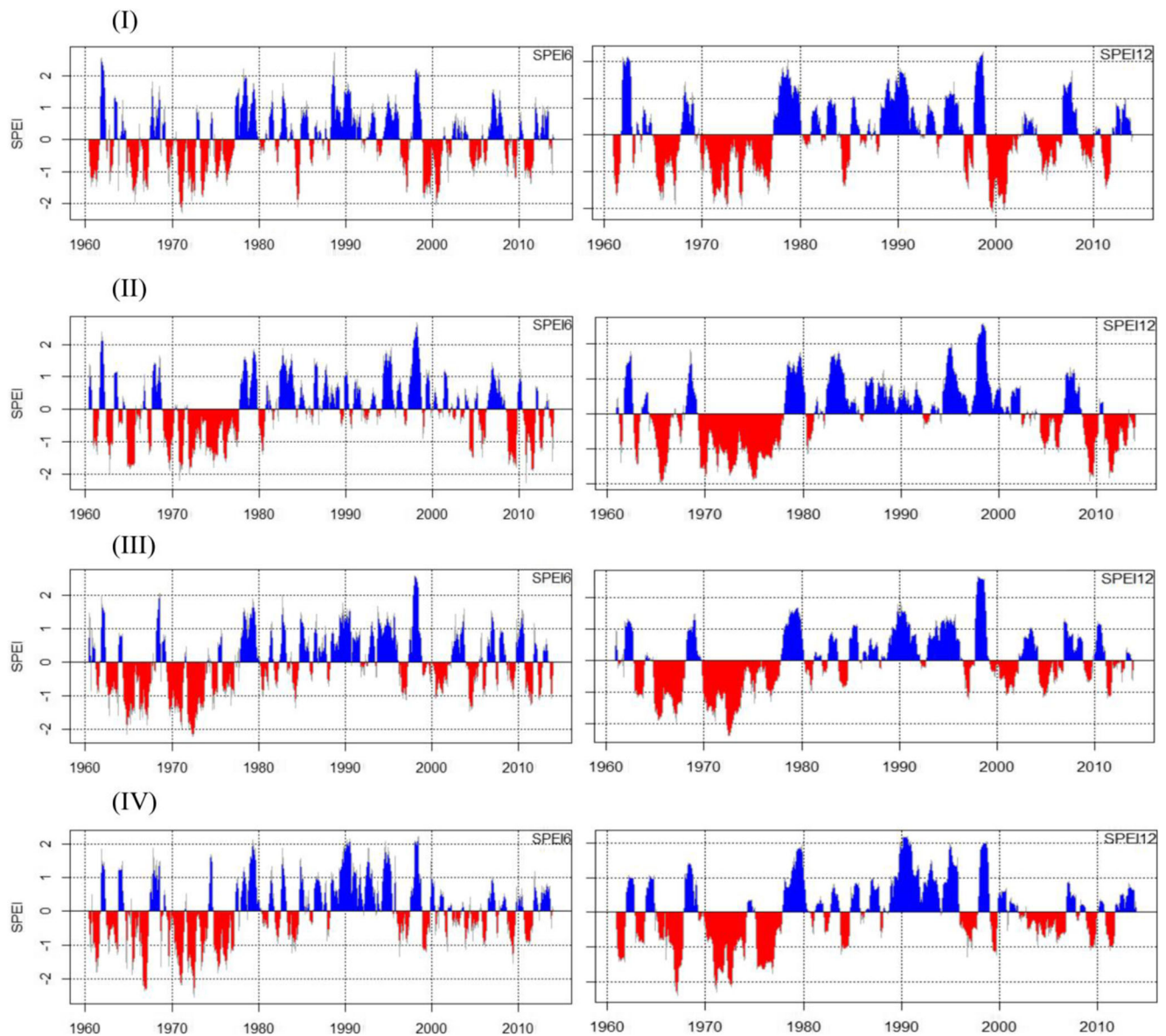
Fig. 4 The evolution of the dry events (red color) and wet events (blue color) for SPEI6 (left panels) and SPEI12 (right panels) over (I) the highlands, (II) coastal, (III) northern and (IV) southern parts of the TRB

dominant factors that affect socio-economic and ecological development. The number of months in which the various categories of events (Table 1) occur during the study period is given in Table 4. It can be seen that on a given timescale, near normal and moderate events occur most frequently and extreme events occur least frequently. The number of extreme dry events ranged from 3 to 16 for SPEI6 and 0 to 19 for SPEI12. The severe dry events occurred in the range of 18 and 49 for SPEI6 and 23 and 48. The occurrence of extreme wet events ranged from 6 to 22 events for SPEI6 and from 7 to 19 events for SPEI12. The prevalence of the of the dry and wet events was investigated for each timescale based on the percentage occurrence of each event (within each

category) for all the grid cells with respect to the total number of months in the same category and timescale. The aim is to identify areas that frequently encounter extreme and severe weather events at comparable timescales, based on their percentage occurrence. The frequency of occurrence is the number of months that the SPEI value attains a set threshold value (see Table 1) divided by the number of months in the entire series. The spatial pattern of the frequency of extreme dry and wet events and severe dry and wet events for the 6- and 12-month timescales is shown in Figs. 5 and 6. The frequency of extreme dry events for SPEI6 ranged from 0.16 (in grid cell 5 and 17) to 2.49% (in grid cells 11, 19 and 31) and 0 to 2.98% for SPEI12. As shown in Fig. 5,

Table 2 The duration, severity and intensity of occurrence of some of the major dry events (SPEI ≤ − 1) in the basin

Grid cell	Period of occurrence	Duration	Severity	Intensity
Dry events for SPEI6				
1	Dec 1973–Apr 1975	17	− 26.27	− 1.56
5	Nov 1964–Oct 1965	12	− 19.42	− 1.62
5	Dec 1973–May 1976	30	− 44.67	− 1.49
16	Sep1964–Sep 1965	13	− 19.72	− 1.52
18	Oct 1971–Oct 1973	25	− 43.07	− 1.72
19	Oct 1971–Oct 1973	25	− 46.21	− 1.85
30	Oct 1970–Sep 1972	24	− 47.2	− 1.97
31	Sep 1970–Sep 1972	25	− 54.54	− 2.18
39	Oct 1964–Jan 1966	16	− 25.14	− 1.57
Dry events for SPEI12				
6	Nov 1969–Jun 1973	44	− 66.23	− 1.51
4	Apr 1074–Jul 1977	40	− 51.2	− 1.28
3	May 1974–Mar 1977	35	− 48.53	− 1.38
18	Nov 1969–Oct 1973	48	− 76.98	− 1.6
19	Nov 1969–Feb 1974	52	− 88.08	− 1.69
20	Dec 1969–Feb 1974	51	− 78.45	− 1.54
23	Aug 1970–Feb 1974	43	− 61.37	− 1.43
25	Aug 1970–Feb 1974	43	− 62.53	− 1.45
31	Oct 1970–Feb 1974	41	− 79.46	− 1.94

Table 3 The duration, severity, and intensity of occurrence of some of the major wet events (SPEI ≥ 1) in the basin

Grid cell	Period of occurrence	Duration	Severity	Intensity
Wet events for SPEI6				
13	May 1982–Mar 1984	23	30.16	1.31
13	Jun 1997–Sep 1998	15	27.84	1.86
14	Jun 1997–Sep 1998	15	28.88	1.93
23	Jul 1997–Sep 1998	15	28.65	1.91
26	Apr 1989–Sep 1990	18	31.75	1.76
29	Apr 1989–Oct 1990	19	28.85	1.52
30	Apr 1989–Sep 1990	18	27.8	1.54
36	Apr 1989–Sep 1990	18	30.76	1.71
37	Apr 1989–Sep 1990	18	33.59	1.87
39	Dec 1988–Oct 1990	23	40.03	1.74
Wet events for SPEI12				
21	Nov 1992–Jan 1996	39	57.22	1.47
25	Jan 1978–Dec 1979	24	37.75	1.57
26	Apr 1989–Nov 1991	32	52.93	1.65
27	Oct 1989–Nov 1991	26	42.91	1.65
29	Feb 1978–Dec 1979	23	36.35	1.58
37	Dec 1988–Mar 1991	28	50.76	1.81
39	Oct 1988–Mar 1991	30	52.45	1.75
40	Oct 1988–Mar 1991	29	40.48	1.41

the frequency of extreme dry events for SPEI6 extended from the southwestern through the middle to northern part of the basin. The extreme wet events were mainly found in the southeastern part (stretching from the coast towards the interior) and the northeast part of the basin. The extreme dry events for SPEI12 showed a high frequency in the northern part of the basin while the extreme wet events had a higher frequency in the northeastern and southeastern parts of the basin. The frequency of occurrence of severe dry events ranged between 2.8 and 7.62% for SPEI6 and 3.61 to 7.54% for SPEI12 as shown in Fig. 6. For SPEI6, the severe dry events had a high frequency of occurrence in the eastern part of the basin while the severe wet events showed a higher frequency of occurrence in the southwestern part and a few isolated grids in the eastern part of the basin. The severe dry events for SPEI12 also affected the eastern part of the basin albeit on a larger scale than the SPEI6 events. The severe wet events showed a high frequency of occurrence in the southwestern and to a less extent, the southern parts of the basin.

3.2 Spatial patterns of SPEI in the TRB

The SPEI series calculated for the 43 grid cells in the basin between 1960 and 2013 were used to analyze for spatial patterns of distribution of dry and wet events based on the principal component analysis (PCA). From the results of the PCA, the first two leading components which altogether accounted for 84% for SPEI6 and 87% for SPEI12, respectively, of the total explained variance were retained. The first principal component PC1 explains 73% and 79% for the two SPEI classes and has spatially homogenous negative values over the whole basin while the second loading showed both positive and negative values across the basin. The second principal component for both timescales explained a smaller percentage of variance (10.3% and 8.2% for SPEI6 and SPEI12 respectively) suggesting that this component represents more localized spatial patterns of SPEI (Santos et al. 2010). This means that it is possible to have extremely dry areas during specific periods, while other areas are wet. The spatial patterns of the factorial loadings obtained from the two PCAs for each timescale are presented in Fig. 7.

The first loading for SPEI6 characterizes the southeastern and the western part of the basin whereas the loading for SPEI12 highlights the middle part. The southeastern part is the area adjoining the Indian Ocean and the western part of the basin encompasses regions of high elevation. These two parts of the basin receive relatively higher rainfall compared with other parts of the basin. The PC1 loading for SPEI12 shows high values in the middle part of the basin. This region is mainly arid and semi-arid with low rainfall and high temperatures. The corresponding PC scores of the loadings for

Table 4 The frequency (number of months in which the different classifications occur) of dry/wet events of SPEI6 and SPEI12 for all the grid cells in the TRB

Grid cell	Extreme dry		Severe dry		Moderate dry		Near normal		Moderate wet	Severe wet			Extreme wet	
	S6	S12	S6	S12	S6	S12	S6	S12	S6	S12	S6	S12	S6	S12
1	3	6	47	37	72	78	422	403	55	67	28	34	16	12
2	3	6	47	37	72	78	422	403	57	67	26	34	16	12
3	2	0	47	42	66	83	417	412	70	62	30	25	11	13
4	4	4	34	39	87	87	414	406	68	75	23	15	13	11
5	1	1	48	47	76	76	422	405	48	68	37	31	11	9
6	2	4	31	36	106	95	397	404	83	73	14	13	10	12
7	2	8	49	44	72	62	409	420	81	89	18	1	12	13
8	3	8	32	33	85	68	409	414	81	88	21	15	12	11
9	3	5	36	37	78	80	425	410	65	77	21	16	15	12
10	13	9	27	35	67	58	434	425	70	80	15	18	17	12
11	16	7	28	41	65	62	431	418	60	71	26	28	17	10
12	8	6	36	39	62	74	429	424	66	49	26	29	16	16
13	3	6	41	33	66	87	413	407	69	50	40	42	11	12
14	4	3	39	42	76	69	430	434	54	47	25	25	15	17
15	7	5	29	41	75	59	430	413	66	82	20	26	16	11
16	5	0	32	41	86	78	412	407	70	83	24	17	14	11
17	1	5	38	34	77	77	405	407	82	84	30	19	10	11
18	8	10	21	28	75	77	419	405	75	80	36	26	9	11
19	16	9	23	28	57	70	426	427	80	62	31	30	10	11
20	7	4	24	33	83	79	407	413	82	72	31	25	9	11
21	9	5	25	28	73	82	422	407	69	73	35	32	10	10
22	9	9	25	25	71	73	427	429	67	52	29	36	15	13
23	5	1	34	48	78	65	417	424	62	52	31	32	16	15
24	4	2	34	35	76	99	415	390	74	68	30	33	10	10
25	7	4	34	31	74	86	415	414	72	59	31	33	10	10
26	12	9	28	33	65	61	416	435	79	56	33	30	10	13
27	12	11	24	32	65	52	419	437	75	60	37	35	11	10
28	15	5	30	40	56	64	437	415	53	65	41	38	11	10
29	13	9	22	31	74	80	431	416	53	52	37	39	13	10
30	10	15	28	23	64	58	428	440	73	61	24	23	16	17
31	16	19	18	26	63	45	450	456	50	61	27	8	19	22
32	9	10	35	26	60	67	435	422	54	66	36	34	14	12
33	12	12	31	32	64	65	429	408	63	73	27	35	17	12
34	9	9	34	26	67	72	421	419	62	67	40	34	10	10
35	9	4	21	27	83	87	417	392	67	84	39	37	7	6
36	11	4	27	41	65	63	420	407	74	81	35	32	11	9
37	13	8	22	33	69	58	420	420	75	73	33	35	11	10
38	10	7	31	37	62	57	421	403	75	87	34	39	10	7
39	11	10	29	31	62	63	431	417	68	69	29	33	13	14
40	7	9	40	30	56	68	427	417	73	70	25	26	15	17
41	4	4	39	44	71	50	430	432	62	77	20	9	17	21
42	9	3	27	34	66	73	433	409	71	78	23	31	14	9
43	11	3	33	43	73	71	423	405	59	67	34	40	10	8

the two timescales are given in Fig. 8. The associated PC1 scores for both timescales describe the temporal behavior of the SPEI in the basin. The scores show a pattern of downward (negative) trend from 1960 to 1995 and thereafter the series
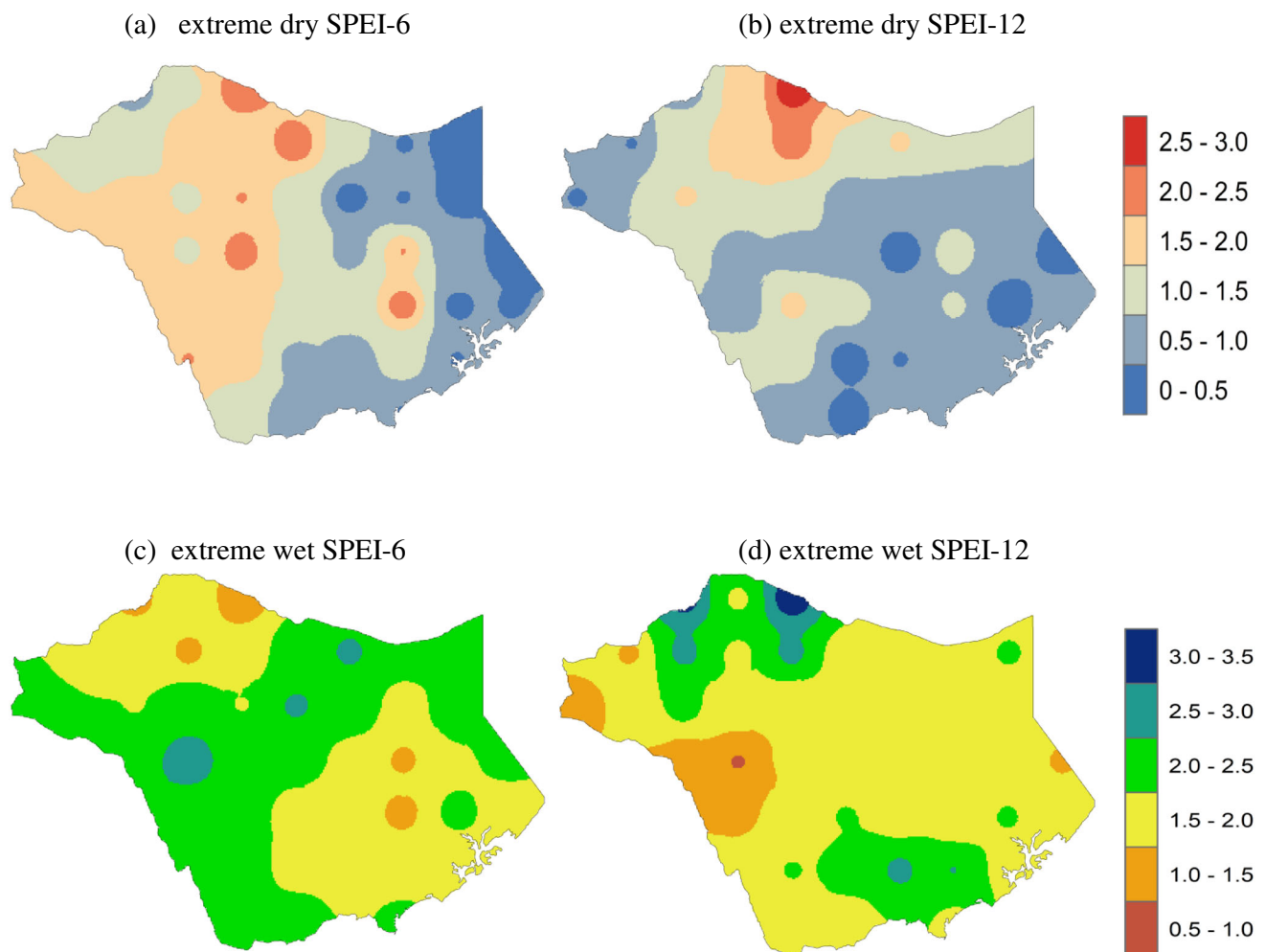
(a) extreme dry SPEI-6

(b) extreme dry SPEI-12

(c) extreme wet SPEI-6

(d) extreme wet SPEI-12

Fig. 5 The spatial pattern of the frequency of extreme dry events (top panel) and extreme wet events (bottom panel) computed for the 6- and 12-month SPEI

stabilizes. The negative values of the PC1 loadings may mean that these regions of the basin have been affected by more frequent dry events. The second PC loading for both timescales is mainly representative of the eastern part of the basin. The second PC scores for SPEI6 show high frequency oscillation without any noticeable trend from 1960 to around 1992 followed by a noticeable upward trend from 1992 to 2000 and henceforth a downward trend to the end of the period. The second PC scores for SPEI12 similarly did not feature any noticeable pattern from 1960 to 1992. Thereafter, there was a noticeable downward trend from 1992 to 2002 and finally a sharp upward trend.

3.3 Wavelet transform of SPEI in TRB

Wavelet transform analysis of the PC scores was performed to show the inter-annual variability of the SPEI in the basin. The wavelet power spectra of the first two PC scores for the two timescales (SPEI6 and SPEI12) are shown in Fig. 9. In this study, the level of significance (confidence) was set to 90%. It

can be seen from Fig. 9 that the wavelet power spectra of PC1 scores for both timescales show similar features. The wavelet transform of the first PC score for both timescales shows significant periodicity between 1 and 2 years between 1960 and 1968, 1970 and 1973, and 1980–1985. There is also a stable inter-decadal higher frequency oscillation at about 2–7 years between 1963 and 1980. In addition, there exists a stable frequency between 1995 and 2010 with oscillations of about 2 to 7 years. Significant periodicities of about 2 to 3 years are distributed in the spectrum of the scores of the second PC and are found between 1960 and 1985 and also 2000 and 2005. Similar results have been found albeit by some studies that undertook a spectral analysis of annual and seasonal rainfall variability over East Africa. A study on trend and periodicity for annual rainfall over East Africa by (Rodhe and Virji 1976) revealed major peaks centered on 2–2.5, 3.5, and 5.6 years. Ogallo (1982) showed the existence of three major peaks, centered on the Quasi-Biennial Oscillation (QBO) of 2.5–3.7 years, ENSO of 4.8–6 years, and the sunspot cycle of 10–12.5 years. Nicholson and Nyenzi (1990) observed a
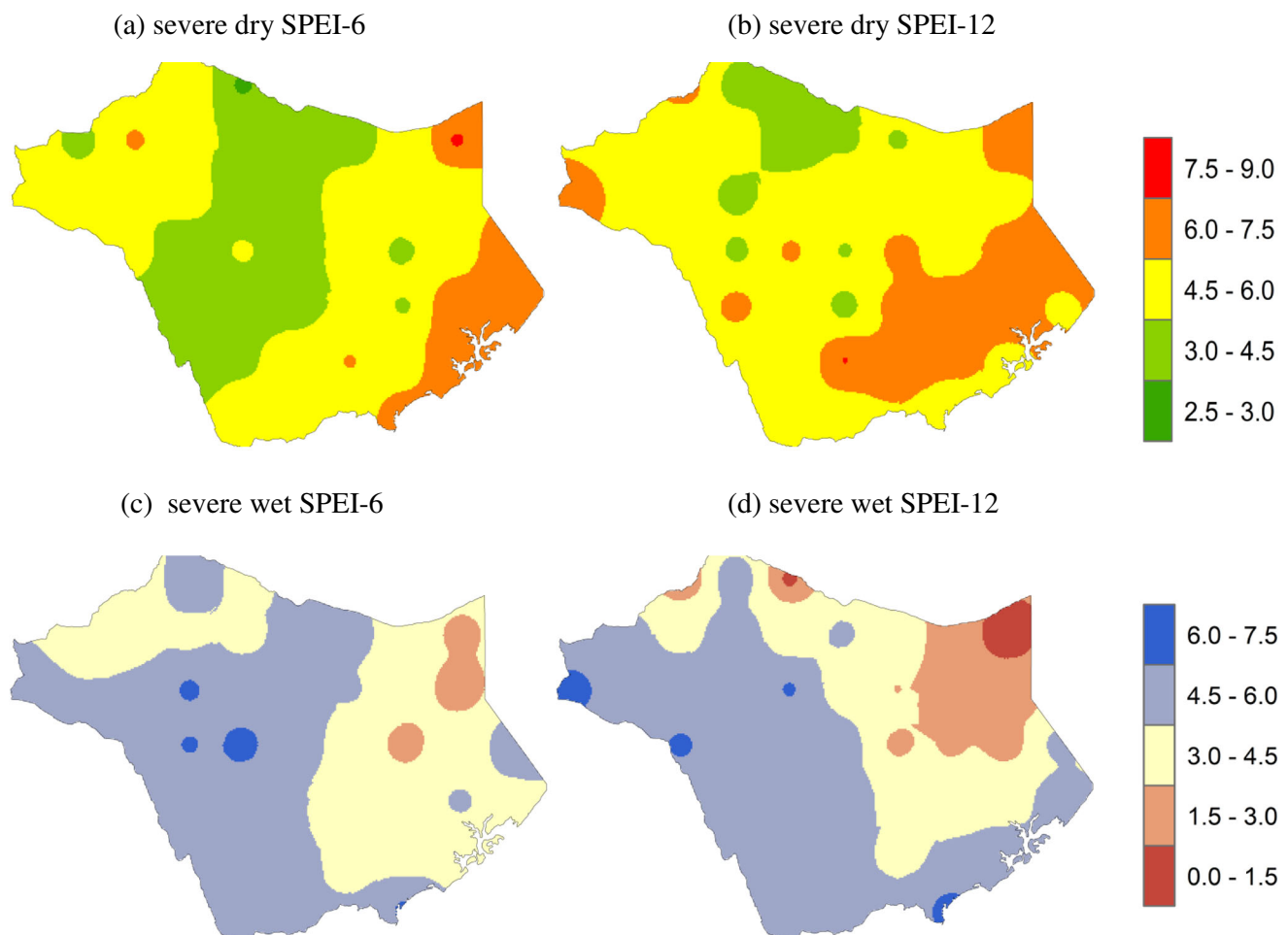
(a) severe dry SPEI-6   (b) severe dry SPEI-12

(c) severe wet SPEI-6   (d) severe wet SPEI-12

Fig. 6 The spatial pattern of the frequency of severe dry events (top panel) and severe wet (bottom panel) events computed for the 6- and 12-month SPEI

strong quasi-periodic fluctuation in the East African rainfall with a timescale of 5–6 years corresponding to the ENSO and sea surface temperatures (SSTs) fluctuations in the equatorial Indian and Atlantic Oceans. A 2–3 year period means that a year with positive SPEI is followed by a year with negative SPEI and then either immediately by a year with positive SPEI or by another year with negative SPEI and then a year with positive SPEI (Hartmann et al. 2012). In addition, a relatively high wavelet power of PC2 of SPEI12 occurred from about 1980 to 1990.

4 Discussion and conclusion

In this study, the characteristics of the extreme weather events over the TRB were investigated based on the 6- and 12-month SPEI for the period beginning 1960 to 2013. It is now accepted that global warming has altered the patterns of rainfall resulting more frequent extreme weather events such as drought and floods. Granted that the TRB ecosystem is highly vulnerable to climate variability and environmental degradation, the SPEI was considered as the most appropriate index because of its

ability to account for potential impacts of climate change in the basin. The spatial and temporal evolution of dry and wet events is captured by both the 6- and 12-month SPEI. It is shown that dry conditions were predominant in the 1960s to 1980s and 2000 to 2013 while wet conditions were experienced between 1980 and 1998. The pattern of the temporal evolution of dry/wet events in the basin can be due to the influence of the high variability of seasonal and annual rainfall in the East African region. Some studies (e.g., Lyon and Dewitt 2012; Shongwe et al. 2011(Lyon 2014)(Lyon 2014)(Lyon 2014)) have suggested that the increase in the frequency of drought conditions post 1998 in the East African region is due to multi-decadal variability of SSTs in the tropical Indian and Pacific oceans. Lyon and Dewitt (2012) observed that the short rains (October–December) in the region showed a robust relationship with the El Niño-Southern Oscillation (ENSO) on the seasonal to interannual timescale while the long rains are mostly linked to sea surface temperature (SSTs) anomalies. Therefore, the high variability of rainfall attributed to La Niña, El Niño, and SSTs could occasion rainfall anomalies leading to decline (or increase) in total seasonal and/or annual rainfall in the basin. For example, the La Niña events significantly contributed to the
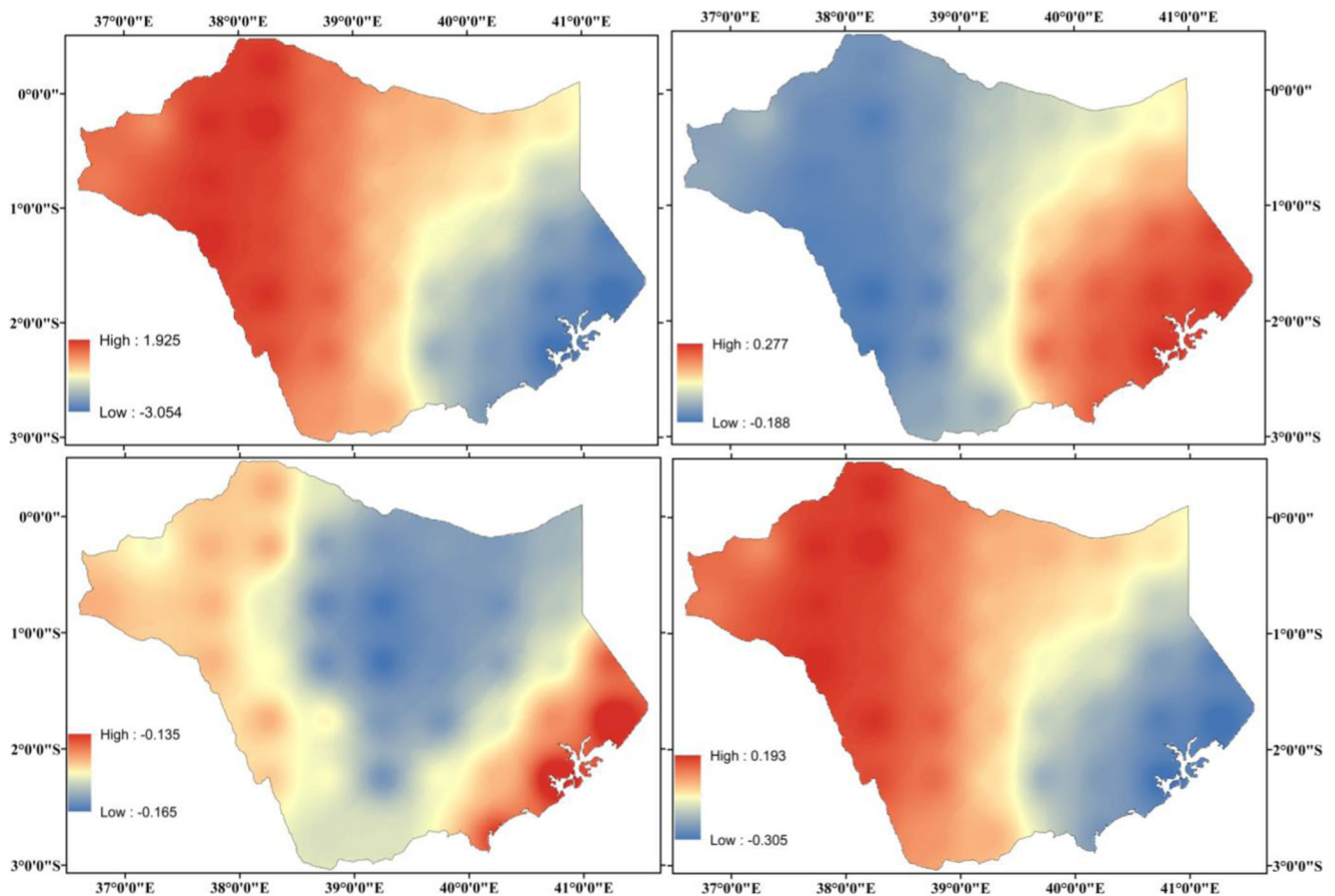
Fig. 7 The spatial pattern of the first two dominant PCA loadings for SPEI6 (top) and SPEI12 (bottom) in the TRB

occurrence of persistent dry events in Kenya in 2010/2011 while El Niño events of 1997 and 1998 caused extreme wet events during that period (Kisaka et al. 2015). This could be the reason for the spatial heterogeneity and non-synchronous occurrence of dry/wet episodes over the basin, where some extreme episodes were witnessed in specific periods over the basin while there were no dry/wet events corresponding to these episodes across other regions of the study domain. The occurrence of long episodes of dry and wet events in the basin is an indication of its susceptibility to climate variability and change.

The PCA analysis revealed a spatial heterogeneity in the 6- and 12-month SPEI variations over the investigated period, with the first two main loadings explaining 84% and 87% of the variability across the basin. In particular, the first loading of the 6-month timescale characterized the southeastern coastal lowlands and the western region of the basin while that for 12-month timescale highlighted the middle part of the basin. These patterns are related to distinct geographical areas and are associated with distinct temporal variations. The leading component of the 12-month SPEI shows that there is a strong relationship between the rainfall distribution and dry/wet events in the region, where the most significant patterns of dry/wet events were specifically found over the coastal and highland regions, while the less significant patterns were

observed over the arid lowlands of the basin. This spatial inhomogeneity of dry/wet events in the basin can be viewed in the context of climate diversity, strong rainfall seasonality, complex topography, and the effects of the Indian Ocean. The long rain (March–May) season is more pronounced in the highlands region while the coastal region usually experiences more enhanced short rains (October–December). The spectral analysis of the PCA loadings shows the influence of these effects on the periodicity of dry/wet events. A periodicity of 2.3 years was reported by Kabanda and Jury (1999) to be dominating the interannual cycle in rainfall variability over Northern Tanzania.

It is evident that the SPEI is a useful tool for analyzing the spatial and temporal pattern of dry and wet conditions in the TRB. Several studies have shown that the index is a valuable tool in the planning and decision-making processes as well as in drought and flood mitigation. The capability of the SPEI in identifying the beginning and end of dry/wet episodes and their spatial variability makes it a potential tool for monitoring hydrological conditions and drought/flood risks given the advantage that it can be calculated at multiple timescales. Although gridded datasets are useful tools for climate variability studies in data scarce regions like Kenya and can be used to complement the scarce observation data, there is need for further
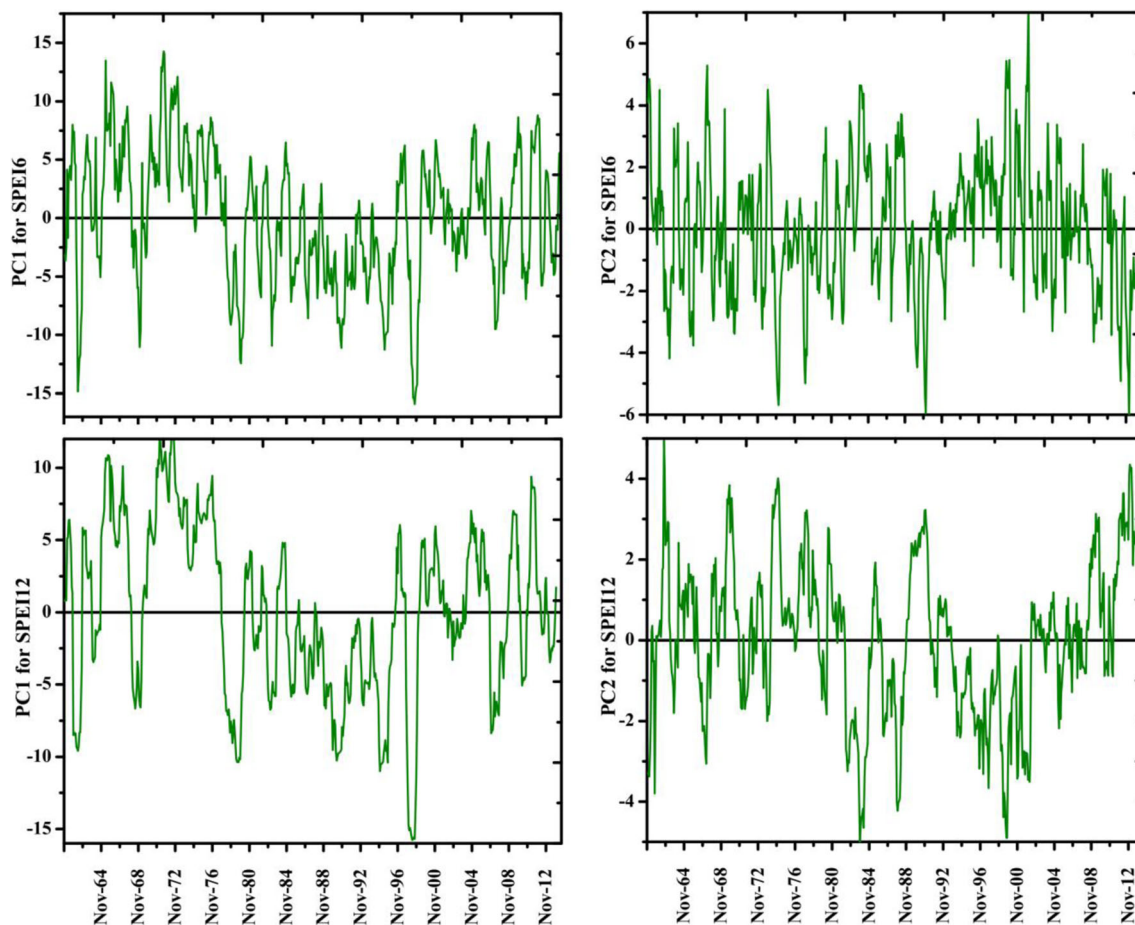
Fig. 8 The temporal pattern of PCA scores corresponding to the first two dominant loading for SPEI6 and SPEI12 in the TRB

studies that utilize high-quality observation data so as to mini-mize the uncertainty problem in analysis. Furthermore, the availability of credible high-quality data will enable exhaustive studies on the effect of temperature change and the atmospheric circulations on the spatial and temporal variability of dry and wet events in the basin. This is because empirical studies (e.g., Vicente-Serrano et al. 2010) have shown that although rainfall is the main variable determining drought/floods conditions, the rise in temperature has important effects on the severity of dry/wet events.
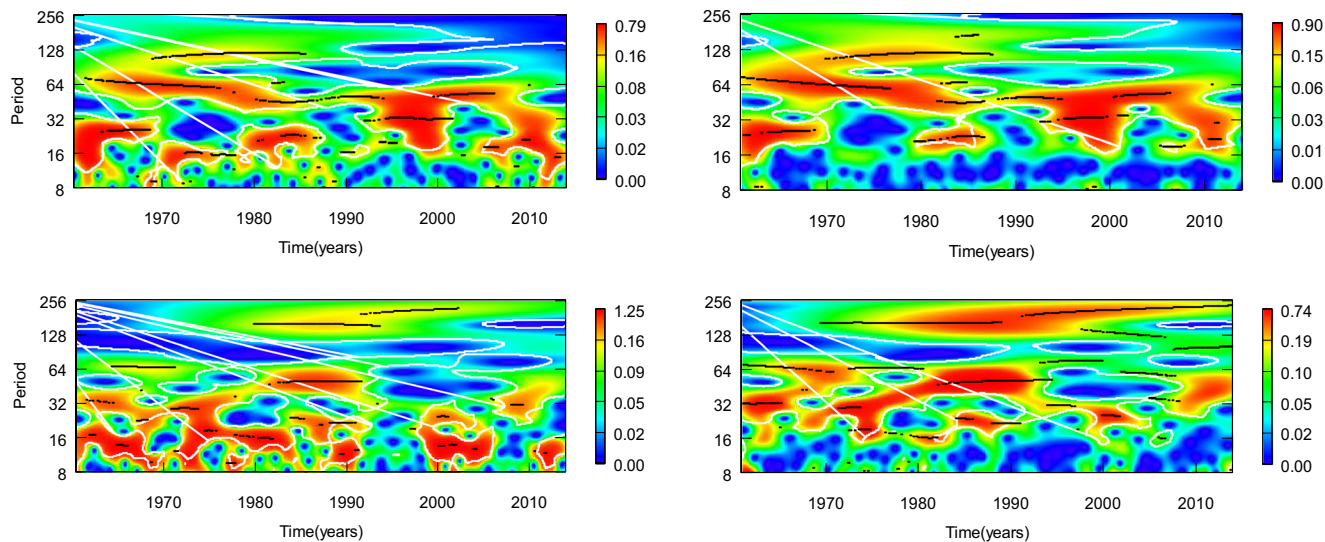
Fig. 9 The continuous wavelet transform of the first two loadings of SPEI6 (top) and SPEI12 (bottom) PC1 and PC2 scores

Compliance with ethical standards

Conflict of interest The authors declare that they have no conflict of interest.

References

Baker T, Kiptala J, Olaka L, Oates N (2015) Baseline review and ecosystem services assessment of the Tana River Basin. IWMI working paper 165, Kenya

Beguería S, Vicente-Serrano SM (2013) Package 'SPEI'. calculation of the Standard Precipitation-Evapotranspiration Index. http://sac.csic.es/spei

Beguería S, Vicente-Serrano SM, Reig F, Latorre B (2014) Standardized precipitation evapotranspiration index (SPEI) revisited: parameter fitting, evapotranspiration models, tools, datasets and drought monitoring. Int J Climatol 34(10):3001–3023. https://doi.org/10.1002/joc.3887

Bordi I, Fraedrich K, Jiang JM, Sutera A (2004) Spatio-temporal variability of dry and wet periods in eastern China. Theor Appl Climatol 79(1–2):81–91. https://doi.org/10.1007/s00704-004-0053-8

Burke EJ, Brown SJ, Christidis N (2006) Modeling the recent evolution of global drought and projections for the twenty-first century with the Hadley Centre climate model. J Hydrometeorol 7(5):1113–1125. https://doi.org/10.1175/JHM544.1

Caramelo L, Orgaz M (2007) A study of precipitation variability in the Duero Basin (Iberian Peninsula). Int J Climatol 27:327–339. https://doi.org/10.1002/joc

Chen H, Sun J (2015) Changes in drought characteristics over China using the standardized precipitation evapotranspiration index. J Clim 28(13):5430–5447. https://doi.org/10.1175/JCLI-D-14-00707.1

Droogers P, Allen RG (2002) Estimating reference evapotranspiration under. Irrig Drain Syst 16:33–45. https://doi.org/10.1023/A:1015508322413

Dubrovsky M, Svoboda MD, Trnka M, Hayes MJ, Wilhite DA, Zalud Z, Hlavinka P (2009) Application of relative drought indices in assessing climate-change impacts on drought conditions in Czechia. Theor Appl Climatol 96(1–2):155–171. https://doi.org/10.1007/s00704-008-0020-x

Gao X, Zhao Q, Zhao X, Wu P, Pan W, Gao X, Sun M (2017) Temporal and spatial evolution of the standardized precipitation evapotranspiration index (SPEI) in the Loess Plateau under climate change from 2001 to 2050. Sci Total Environ 595:191–200. https://doi.org/10.1016/j.scitotenv.2017.03.226

Gichuki, P., & Vigerstol, K. (2014). Presentation from the 2014 world water week in Stockholm

Githui F, Gitau W, Bauwens W (2009) Climate change impact on SWAT simulated streamflow in western Kenya. Int J Climatol 1834(December 2008):1823–1834. https://doi.org/10.1002/joc

Hargreaves GH, Allen RG (2003) History and evaluation of Hargreaves evapotranspiration equation. J Irrig Drain Eng-Asce 129(1):53–63. https://doi.org/10.1061/(ASCE)0733-9437(2003)129:1(53)

Hartmann H, Becker S, Jiang T (2012) Precipitation variability in the Yangtze River subbasins. Water Int 37(1):16–31. https://doi.org/10.1080/02508060.2012.644926

Hayes MJ, Svoboda M, LeComte D, Redmond KT, Pasteris P (2005) Drought monitoring: new tools for the 21st century. In: Wilhite D (ed) Drought and water crises: science, technology, and management issues. CRC Press

Hernandez EA, Uddameri V (2014) Standardized precipitation evaporation index (SPEI)-based drought assessment in semi-arid south Texas. Environ Earth Sci 71(6):2491–2501. https://doi.org/10.1007/s12665-013-2897-7

Hisdal H, Tallaksen LM (2003) Estimation of regional meteorological and hydrological drought characteristics: a case study for Denmark. J Hydrol 281(3):230–247. https://doi.org/10.1016/S0022-1694(03)00233-6

Huang J, Zhang J, Zhang Z, Sun S, Yao J (2012) Simulation of extreme precipitation indices in the Yangtze River basin by using statistical downscaling method (SDSM). Theor Appl Climatol 108(3–4):325–343. https://doi.org/10.1007/s00704-011-0536-3

IPCC (2007) Climate change 2007: the physical science basis. Contribution of working group I to the fourth assessment report of the intergovernmental panel on climate change. J Chem Inf Model 53. https://doi.org/10.1017/CBO9781107415324.004

Jacobs JH, Angerer J, Vitale J, Srinivasan R, Kaitho R (2007) Mitigating economic damage in Kenya's upper Tana River Basin: an application of arc-view SWAT. J Spat Hydrol 7(1):23–46

Jury MR (2010) Ethiopian decadal climate variability. Theor Appl Climatol 101(1):29–40. https://doi.org/10.1007/s00704-009-0200-3

Kabanda TA, Jury MR (1999) Inter-annual variability of short rains over northern Tanzania. Clim Res 13(3):231–241. https://doi.org/10.3354/cr013231

Kerandi NM, Laux P, Arnault J, Kunstmann H (2016) Performance of the WRF model to simulate the seasonal and interannual variability of hydrometeorological variables in East Africa: a case study for the Tana River basin in Kenya. Theor Appl Climatol 130:1–18. https://doi.org/10.1007/s00704-016-1890-y

Kisaka MO, Mucheru-Muna M, Ngetich FK, Mugwe JN, Mugendi D, Mairura F (2015) Rainfall variability, drought characterization, and efficacy of rainfall data reconstruction: case of Eastern Kenya. Adv Meteorol 2015:1–16. https://doi.org/10.1155/2015/380404

Łabedzki L (2007) Estimation of local drought frequency in Central Poland using the standardized precipitation index SPI. Irrig Drain 56:67–77. https://doi.org/10.1002/ird

Lau K-M, Weng H (1995) Climate signal detection using wavelet Transform: How to Make a Time Series Sing. Bull Am Meteorol Soc. https://doi.org/10.1175/1520-0477(1995)076<2391:CSDUWT>2.0.CO;2

Liebmann B, Hoerling MP, Funk C, Blade´ I, Dole RM, Allured D, Quan X, Pegion P, Eischeid JK (2014) Understanding recent Eastern Horn of Africa rainfall variability and change. J Clim 27:8630–8645. https://doi.org/10.1175/JCLI-D-13-00714.1

Liu X, Wang S, Zhou Y, Wang F, Li W, Liu W (2015) Regionalization and spatiotemporal variation of drought in China based on standardized precipitation evapotranspiration index (1961-2013). Adv Meteorol 2015:1–18. https://doi.org/10.1155/2015/950262

Lorenzo-lacruz J, Vicente-serrano SM, López-moreno JI, Beguería S, García-ruiz JM (2010) The impact of droughts and water management on various hydrological systems in the headwaters of the Tagus River (central Spain). J Hydrol 386(1–4):13–26. https://doi.org/10.1016/j.jhydrol.2010.01.001

Lyon B (2014) Seasonal drought in the Greater Horn of Africa and its recent increase during the March-May long rains. J Clim 27(21): 7953–7975. https://doi.org/10.1175/JCLI-D-13-00459.1

Lyon B, Dewitt DG (2012) A recent and abrupt decline in the East African long rains. Geophys Res Lett 39(2):1–5. https://doi.org/10.1029/2011GL050337

Mahfouz P, Mitri G, Jazi M, Karam F (2016) Investigating the temporal variability of the standardized precipitation index in Lebanon. Climate 4(2):27. https://doi.org/10.3390/cli4020027

Mwale D, Gan TY (2004) Wavelet analysis of variability, teleconnectivity, and predictability of the September–November east african rainfall. Journal of Applied Meteorology 44:256–269

Nakaegawa T, Wachana C (2012) First impact assessment of hydrological cycle in the Tana River Basin, Kenya, under a changing climate in the late 21st century. Hydrol Res Lett 6:29–34. https://doi.org/10.3178/hrl.6.29

Nicholson SE, Nyenzi BS (1990) Temporal and spatial variability of SSTs in the tropical Atlantic and Indian oceans. Meteorog Atmos Phys 42(12):1–17. https://doi.org/10.1016/S0198-0254(06)80174-3

Ogallo LJ (1982) Quasi-periodic patterns in the East African rainfall records. *Ken va*. J Sci Technol 3:43–54

Okazawa H, Toyoda H, Suzuki S, Shimada S, Nishimaki R (2009) Long-term discharge analysis using the EPA method for the Tana River in Kenya. J Arid Land Stud 19:57–60

Oludhe C, Sankarasubramanian A, Sinha T, Devineni N, Lall U (2013) The role of multimodel climate forecasts in improving water and energy management over the Tana River Basin, Kenya. J Appl Meteorol Climatol 52(11):2460–2475. https://doi.org/10.1175/JAMC-D-12-0300.1

Ongoma V, Chen H (2017) Temporal and spatial variability of temperature and precipitation over East Africa from 1951 to 2010. Meteorol Atmos Phys 129:131–144. https://doi.org/10.1007/s00703-016-0462-0

Potop V, Možný M, Soukup J (2012) Drought evolution at various time scales in the lowland regions and their impact on vegetable crops in the Czech Republic. Agric For Meteorol 156:121–133. https://doi.org/10.1016/j.agrformet.2012.01.002

Rajeevan M, Bhate J, Kale JD, Lal B (2006) High resolution daily gridded rainfall data for the Indian region: analysis of break and active monsoon spells. Curr Sci 91(3):296–306. https://doi.org/10.1007/s12040-007-0019-1

Raziei T, Bordi I, Pereira LS (2011) An application of GPCC and NCEP/NCAR datasets for drought variability analysis in Iran. Water Resour Manag 25(4):1075–1086. https://doi.org/10.1007/s11269-010-9657-1

Rodhe H, Virji H (1976) Trends and periodicities in East African rainfall data. Mon Weather Rev 104(March 1976):307–315. https://doi.org/10.1175/1520-0493(1976)104<0307:TAPIEA>2.0.CO;2

Rosch A, Schmidbauer H (2014) WaveletComp : a guided tour through the R-package, 1–38

Rowell DP, Booth BBB, Nicholson SE, Good P (2015) Reconciling past and future rainfall trends over East Africa. J Clim 28(24):9768–9788. https://doi.org/10.1175/JCLI-D-15-0140.1

Santos CA, Ideião SM (2005) Application of the wavelet transform for analysis of precipitation and runoff time series. Predictions in Ungauged Basins: Promise and Progress (Proceedings of symposium S7 held during the Seventh IAHS Scientific Assembly at Foz do Iguaçu, Brazil, April 2005). IAHS Publ. 303, 2006

Santos JF, Pulido-Calvo I, Portela MM (2010) Spatial and temporal variability of droughts in Portugal. Water Resour Res 46(3):1–13. https://doi.org/10.1029/2009WR008071

Schneider U, Becker A, Finger P, Meyer-Christoffer A, Ziese M, Rudolf B (2014) GPCC's new land-surface precipitation climatology based on quality-controlled in-situ data and its role in quantifying the global water cycle, Theor Appl Climatology 115:15–40. https://doi.org/10.1007/s00704-013-0860-x; http://link.springer.com/article/10.1007%2Fs00704-013-0860-x

Shi B, Zhu X, Hu Y, Yang Y (2017) Drought characteristics of Henan province in 1961-2013 based on standardized precipitation evapotranspiration index. J Geogr Sci 27(3):311–325. https://doi.org/10.1007/s11442-017-1378-4

Shongwe ME, van Oldenborgh GJ, van den Hurk B, van Aalst M (2011) Projected changes in mean and extreme precipitation in Africa under global warming. Part II: East Africa. J Clim 24(14):3718–3733. https://doi.org/10.1175/2010JCLI2883.1

Stagge J, Tallaksen L (2014) Standardized precipitation-evapotranspiration index (SPEI): sensitivity to potential evapotranspiration model and parameters. Int Assoc Hydrol Sci (IAHS) 10(October):367–373 Retrieved from http://www.researchgate.net/profile/Chong_Yu_Xu/publication/270576580_Standardized_precipitation-evapotranspiration_index_(SPEI)_Sensitivity_to_potential_evapotranspiration_model_and_parameters/links/54b386240cf220c63cd2836a.pdf. Accessed 16 Feb 2018

The World Bank (2011) The drought and food crisis in the horn of africa

Torrence C, Compo GP (1998) A practical guide to wavelet analysis. Bull Am Meteor Soc 79(1):61–78. https://doi.org/10.1175/1520-0477(1998)079<0061:APGTWA>2.0.CO;2

Vicente-serrano SM, Beguería S, López-moreno JI, Juan I (2010) A multiscalar drought index sensitive to global warming : the standardized precipitation evapotranspiration index. J Clim 23:1696–1718. https://doi.org/10.1175/2009JCLI2909.1

Vicente-Serrano SM, Beguería S, Lorenzo-Lacruz J, Camarero JJ, López-Moreno JI, Azorin-Molina C et al (2012) Performance of drought indices for ecological, agricultural, and hydrological applications. Earth Interact 16(10):1–27. https://doi.org/10.1175/2012EI000434.1

Wagesho N, Goel NK, Jain MK (2013) Temporal and spatial variability of annual and seasonal rainfall over Ethiopia. Hydrol Sci J 58(2):354–373. https://doi.org/10.1080/02626667.2012.754543

Wambua RM, Mutua BM, Raude JM (2015) Spatio-temporal drought characterization for the upper Tana River Basin, Kenya using Standardized Precipitation Index (SPI). World Journal of Environmental Engineering 3(4):111–120. https://doi.org/10.12691/wjee-3-4-2

Williams AP, Funk C (2011) A westward extension of the warm pool leads to a westward extension of the Walker circulation , drying Eastern Africa. Clim Dyn 37(2011):2417–2435. https://doi.org/10.1007/s00382-010-0984-y

Worqlul AW, Maathuis B, Adem AA, Demissie SS, Langan S, Steenhuis TS (2014) Comparison of rainfall estimations by TRMM 3B42, MPEG and CFSR with ground-observed data for the Lake Tana basin in Ethiopia. Hydrol Earth Syst Sci 18(12):4871–4881. https://doi.org/10.5194/hess-18-4871-2014

Wu C, Xian Z, Huang G (2016) Meteorological drought in the Beijiang River basin, South China: current observations and future projections. Stoch Environ Res Risk Assess 30:1821–1834. https://doi.org/10.1007/s00477-015-1157-7

Yu M, Li Q, Hayes MJ, Svoboda MD, Heim RR (2014) Are droughts becoming more frequent or severe in China based on the standardized precipitation evapotranspiration index: 1951-2010? Int J Climatol 34(3):545–558. https://doi.org/10.1002/joc.3701

Zambreski ZT (2016) A stastical assessment of drought variability and climate prediction for Kansas. A Master Degree Thesis for Kansas State University

Zhang Q, Xu C, Zhang Z (2009) Observed changes of drought / wetness episodes in the Pearl River basin, China, using the standardized precipitation index and aridity index. Theor Appl Climatol 98:89–99. https://doi.org/10.1007/s00704-008-0095-4

Zhao G, Mu X, Hörmann G, Fohrer N, Xiong M, Su B (2012) Spatial patterns and temporal variability of dryness/wetness in the Yangtze River. Quat Int 282:5–13. https://doi.org/10.1016/j.quaint.2011.10.020